

Supplementary Information

Unraveling the Mechanism of a LOV Domain Optogenetic Sensor: A Glutamine Lever Induces Unfolding of the Ja Helix

James N. Iuliano,[†] Jinnette Tolentino Collado,[†] Agnieszka A. Gil,[‡] Pavithran T. Ravindran,[‡] Andras Lukacs,^{‡,§} SeungYoun Shin,[†] Helena A. Woroniecka,[†] Katrin Adamczyk,[‡] James M. Aramini,[¶] Uthama R. Edupuganti,^{¶,§} Christopher R. Hall,[‡] Gregory M. Greetham,^{||} Igor V. Sazanovich,^{||} Ian P. Clark,^{||} Taraneh Daryaee,[†] Jared E. Toettcher,[‡] Jarrod B. French,^{†,±} Kevin H. Gardner,^{¶,&,#} Carlos Simmerling,^{†*} Stephen R. Meech,^{‡*} and Peter J. Tonge.^{†*}

[†]Department of Chemistry, Stony Brook University, New York, 11794, United States. [‡]Department of Molecular Biology, Princeton University [§]School of Chemistry, University of East Anglia, Norwich, NR4 7TJ, U.K. [§]Department of Biophysics, Medical School, University of Pecs, Szigetesi út 12, 7624 Pecs, Hungary. ^{||}Central Laser Facility, Research Complex at Harwell, Rutherford Appleton Laboratory, Didcot, OX11 0QX, U.K. [¶]Structural Biology Initiative, CUNY Advanced Science Research Center, 85 St. Nicholas Terrace, New York, NY 10031. [¶]Ph.D. Program in Biochemistry, CUNY Graduate Center, New York, NY; [&]Ph.D. Programs in Biochemistry, Biology, and Chemistry, CUNY Graduate Center, New York, NY; [#]Department of Chemistry & Biochemistry, City College of New York, New York, NY; [±]Hormel Institute, University of Minnesota, Austin, MN, 55912.

*Authors to whom correspondence should be addressed:

Email: carlos.simmerling@stonybrook.edu (CLS); s.meech@uea.ac.uk (SRM);

peter.tonge@stonybrook.edu (PJT)

Keywords: LOV, structural dynamics, optogenetics, flavoprotein, ultrafast IR

Table of Contents

	Page
Figure S1. Undocking of the J α helix.	3
Figure S2: Comparison of light-state crystal structure and 6.8 μ s MD simulation.	4
Figure S3: Dark State molecular dynamics simulation shows stability of the J α helix.	5
Figure S4: Light-Dark FTIR Shows reduced helix unfolding in N414A-AsLOV2.	6
Figure S5: Evolution of difference spectrum on the 100s of μ s timescale shows full structural changes in AsLOV2.	7
Figure S6: Kinetics of the C4a=C10a vibrational mode does not decay on the timescale of the experiment.	8
Figure S7: Selected traces showing quality of the global fitting.	9
Figure S8: HSQC NMR of WT AsLOV2 in both dark and light states.	10
Figure S9: HSQC NMR of N414A AsLOV2 in both dark and light states.	11
Figure S10: HSQC NMR of N414Q AsLOV2 in both dark and light states.	12
Figure S11: Fitting of the recovery traces from the LOVTRAP assay.	13
Figure S12: Comparison of 5d-FMN-Aureo with AsLOV2.	14
Figure S13: Alignment of LOV domain proteins.	15

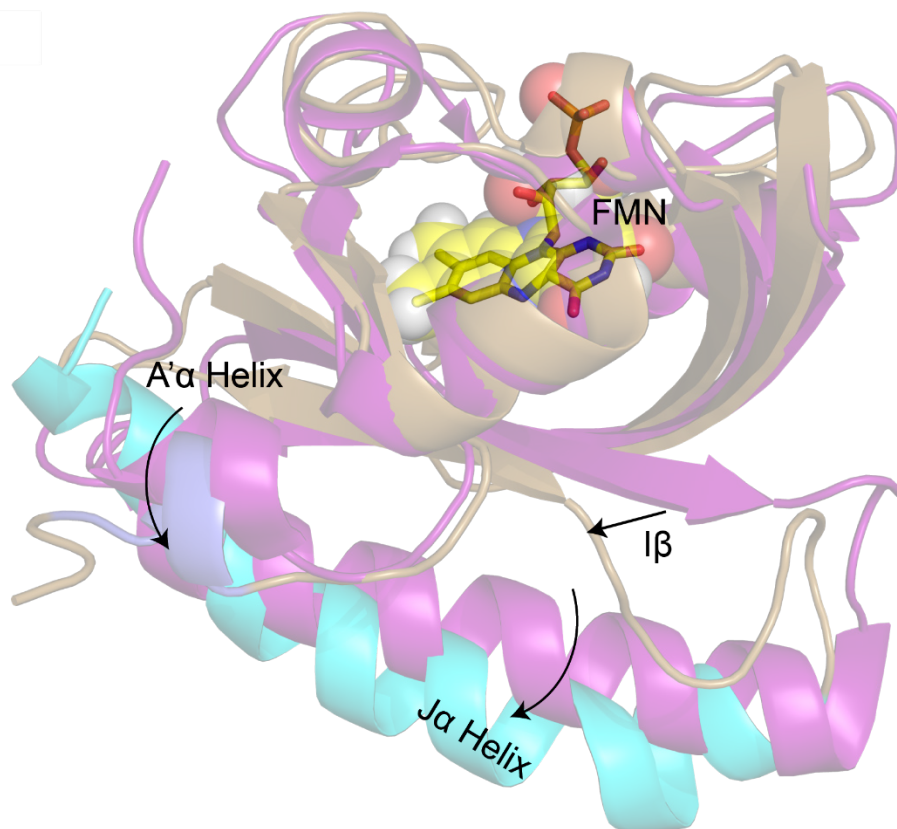


Figure S1: Initial events of the J α helix unfolding. (A) The J α helix is predicted to begin to undock $\sim 0.5 \mu\text{s}$ after adduct formation. The dark state structure 2V1A is shown in magenta for reference. I β and the hinge loop region become more disordered allowing the J α helix to begin to adopt an undocked conformation (cyan) and move away from the β -sheet (brown). The figure was made using the PyMOL Molecular Graphics System, Version 1.8, Schrödinger LLC.²⁰

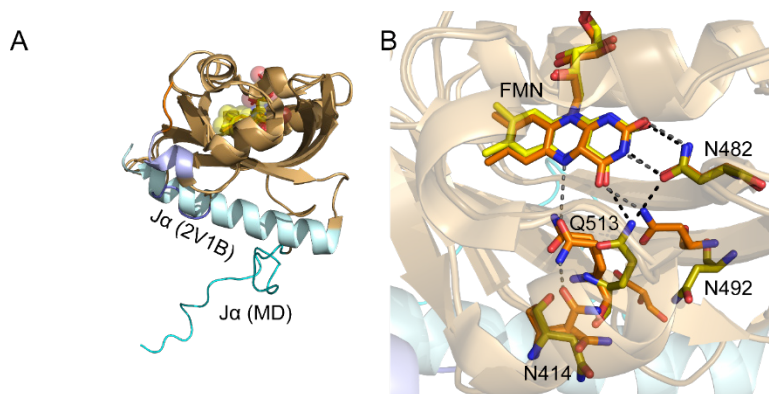


Figure S2: Comparison of light-state X-ray structure and the structure formed after 6.8 μ s of MD simulation. (A) Helix (cyan) unfolding is not observed in the light state structure (2V1B) due to crystal contacts but in the absence of these constraints becomes disordered following MD. (B) Increased mobility of the FMN H-bond network is predicted by MD simulations (gold) in which N492 is predicted to remain out of the pocket, 4 Å displaced from the position from the crystal structure (orange). The figure was made using the PyMOL Molecular Graphics System, Version 1.8, Schrödinger LLC.²⁰

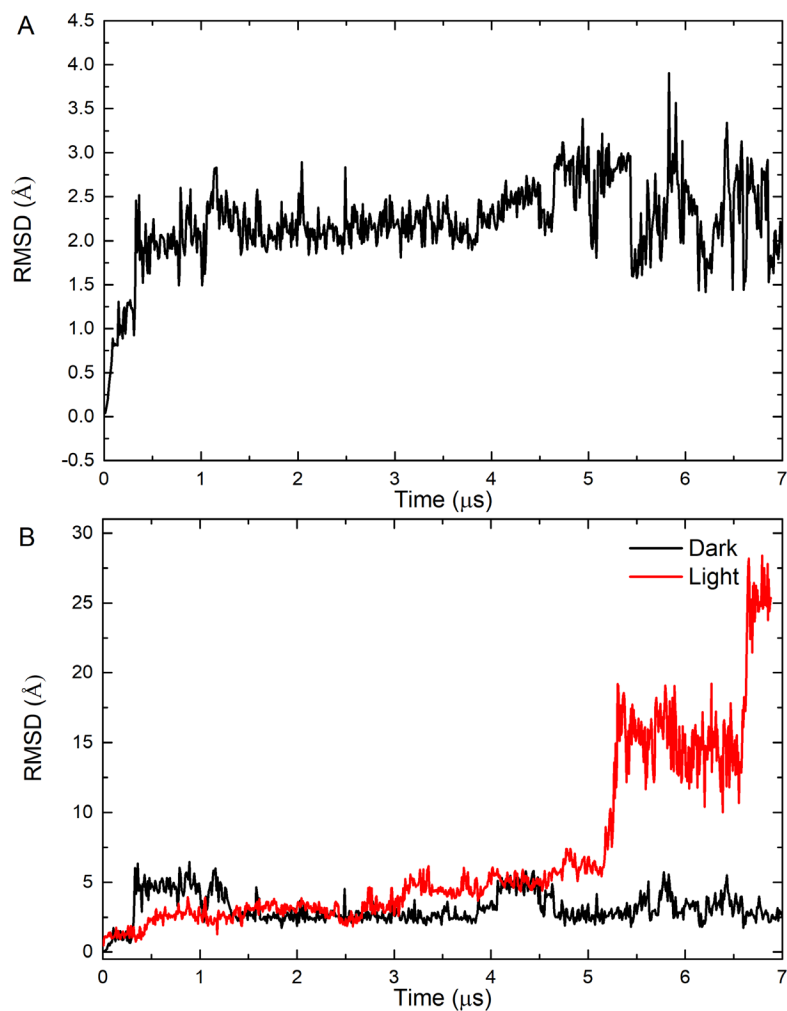


Figure S3: Dark state molecular dynamics simulation shows stability of the J α helix. The RMSD vs. time was plotted for residues corresponding to (A) the entire protein including the J α helix and (B) the J α helix alone compared to the light state J α helix.

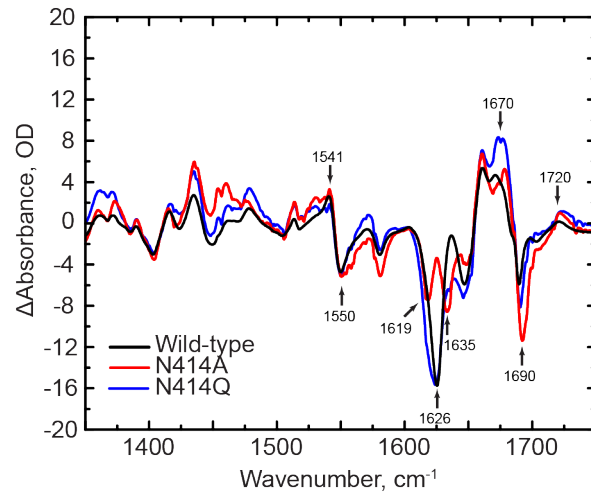


Figure S4: Light-Dark FTIR Spectra of N414A-AsLOV2. L-D FTIR difference spectra show full helix unfolding in WT-AsLOV2 and N414Q-AsLOV2 and reduced helix unfolding in N414A-AsLOV2 mutant. The marker band for the J α helix is observed at 1626 cm⁻¹.

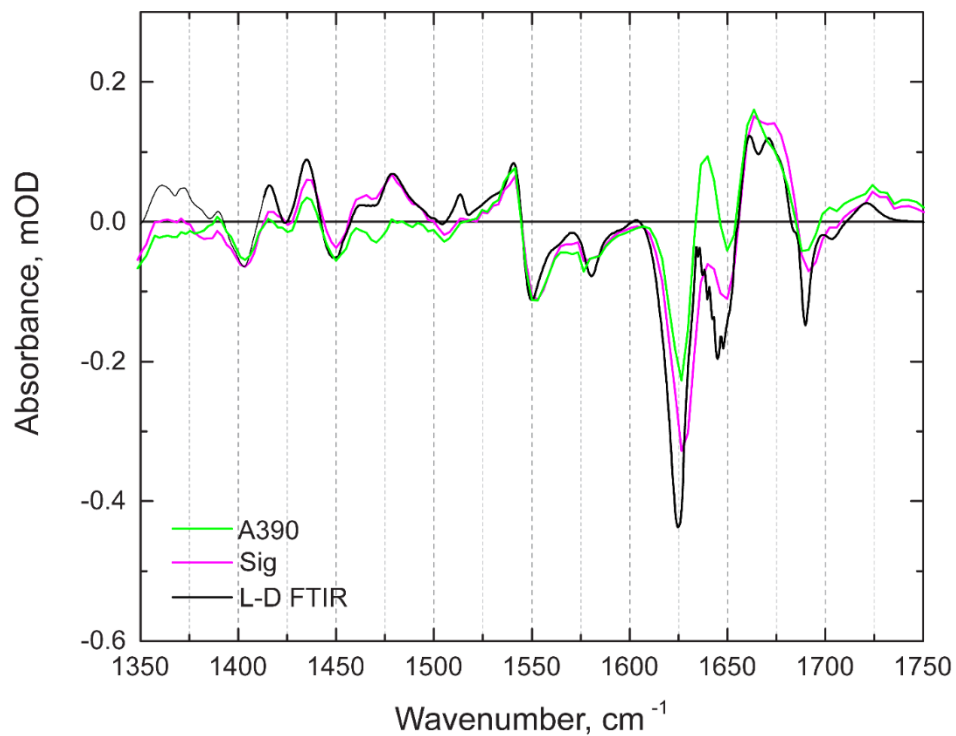


Figure S5: Evolution of the FTIR difference spectrum on the 100s of μ s timescale. The full extent of the structural changes in wild-type AsLOV2 are shown by comparison of the light – dark FTIR difference spectrum (L-D FTIR, black) with EAS from a global fit of the TRMPS spectra corresponding to adduct formation (14 μ s, A390 in green) and formation of the final signaling state (313 μ s, Sig in purple). This data shows that full light state formation is captured in the TRMPS experiment.

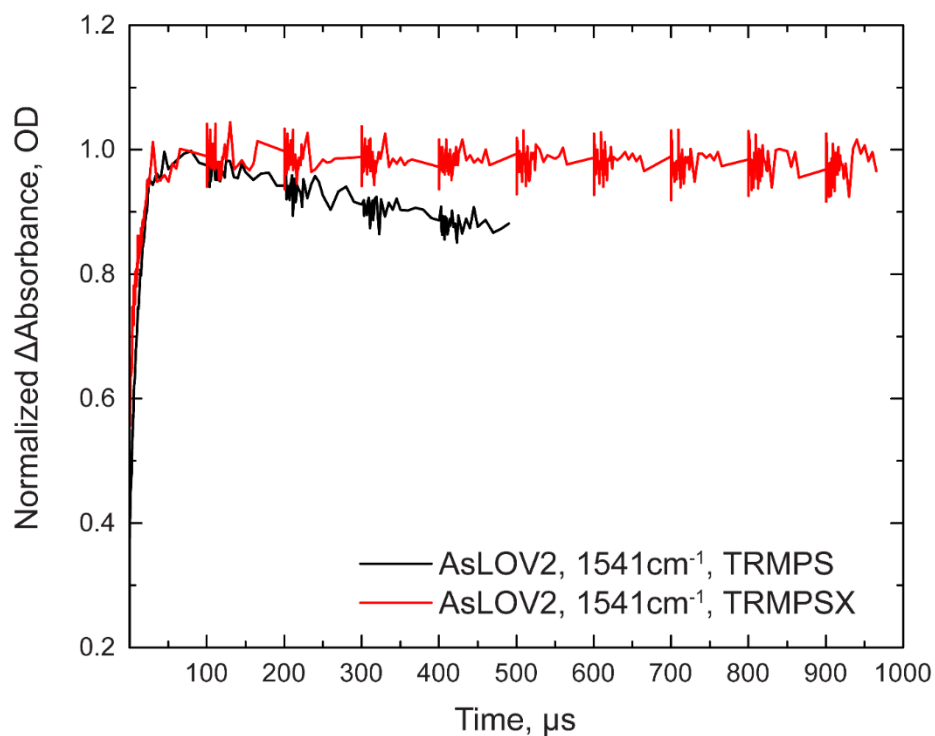


Figure S6: Kinetics of the C4a=C10a vibrational mode from TRMPS and TRMPSX. In the standard TRMPS experiment, a pump-off subtraction is taken at the final probe pulse and assumes that all signals are decayed by 1 ms. For AsLOV2 (and LOV in general), the light state is stable on the order of seconds such that signals from the light state are subtracted at later time delays. Employing the TRMPSX method and lowering the pump laser repetition rate to 500 Hz allows for a pump-off subtraction to be acquired at 2 ms, allowing for sufficient time for sample refresh prior to the pump-off pulse. The above traces compare the evolution of the 1541 cm^{-1} transient assigned to the C4a=C10a vibrational mode from FMN acquired using TRMPS and TRMPSX. The signals acquired using TRMPSX do not decay on the ms timescale allowing for analysis of signals beyond 100 μs .

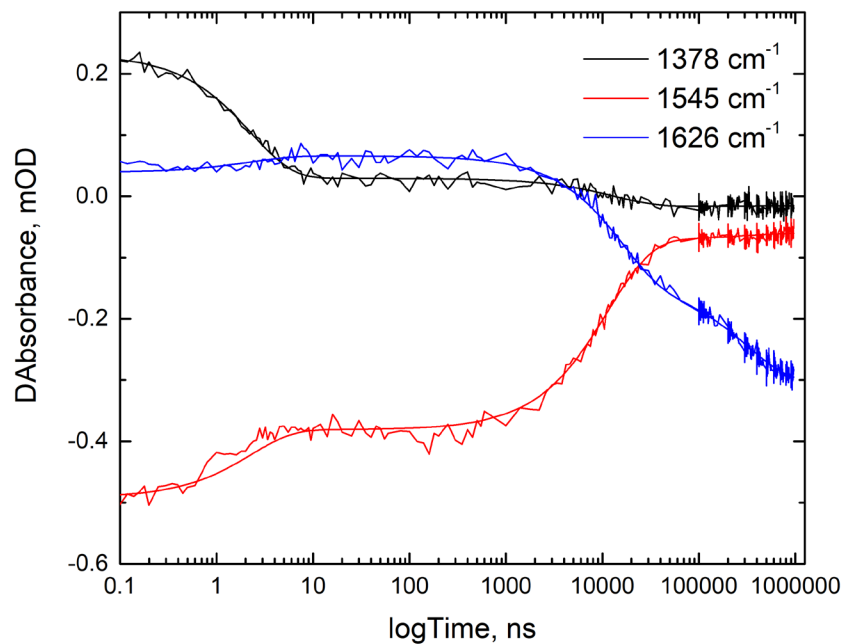


Figure S7: Selected time traces showing quality of the global fitting. Global fitting of the TRMPSX datasets to a sequential exponential model containing 5 components was used to extract time constants for the phases of evolution of AsLOV2 from dark to light state. Signals corresponding to excited state decay (1378 cm⁻¹), ground state recovery (1545 cm⁻¹), and the J α helix (1626 cm⁻¹) are shown as representative kinetic traces.

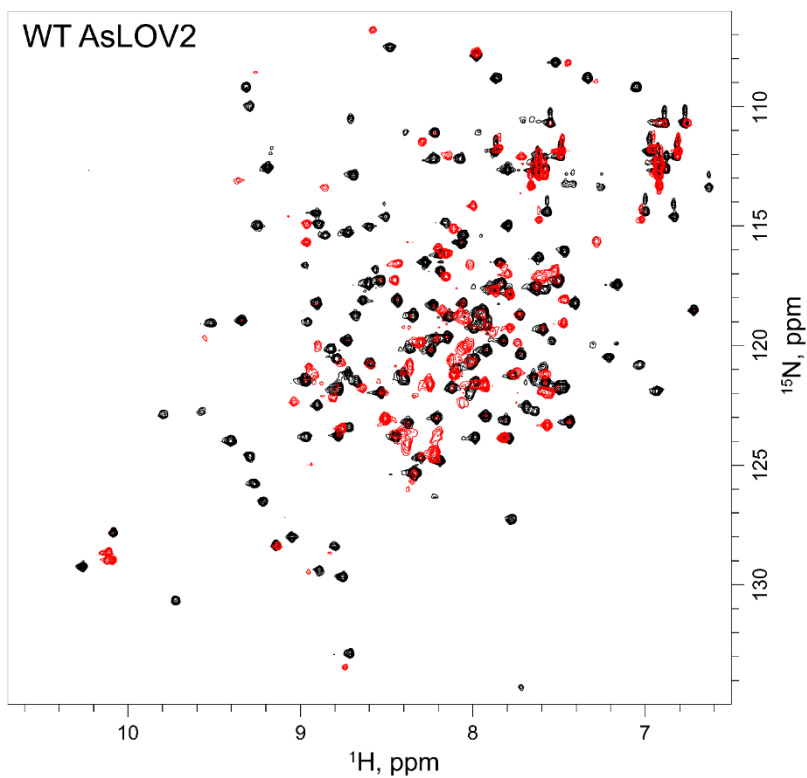


Figure S8: ^1H - ^{15}N -HSQC NMR spectra of wild-type AsLOV2. 800 MHz NMR spectra of ^{15}N labeled WT-AsLOV2 in the dark (black) and light states (red) are shown. The light state was generated by irradiation with 50 mW, 120ms pulse duration of 488 nm light prior to collecting each transient spectrum. Data were processed and analyzed using Bruker TopSpin.

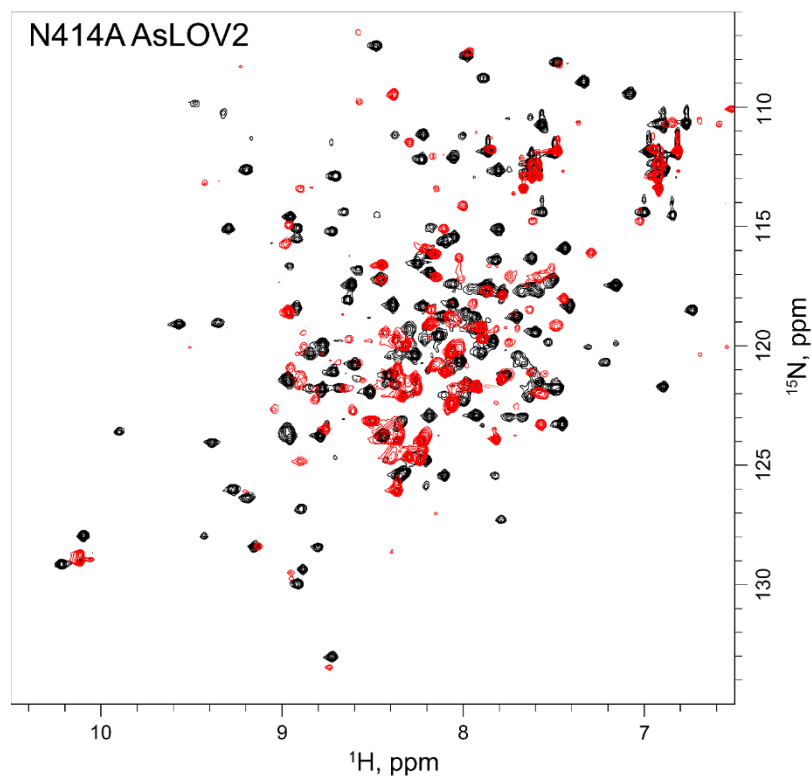


Figure S9: ^1H - ^{15}N -HSQC NMR spectra of N414A AsLOV2. 800 MHz NMR spectra of ^{15}N labeled N414A-AsLOV2 in the dark (black) and light states (red) are shown. The light state was generated by irradiation with 50 mW, 120ms pulse duration of 488 nm light prior to collecting each transient spectrum. Data were processed and analyzed using Bruker TopSpin.

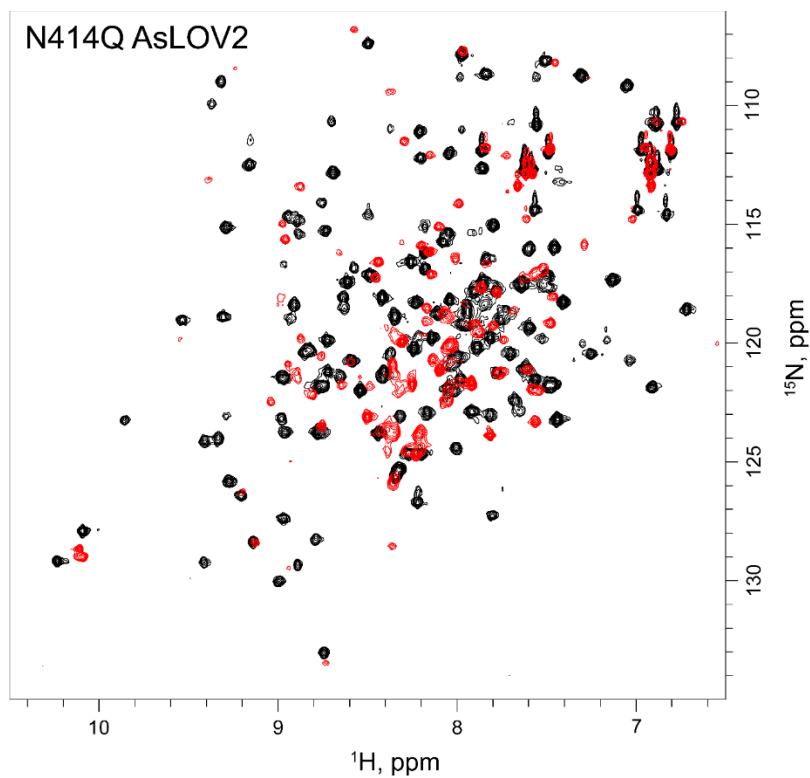


Figure S10: ^1H - ^{15}N -HSQC NMR spectra of N414Q-AsLOV2. 800 MHz NMR spectra of ^{15}N labeled N414Q-AsLOV2 in the dark (black) and light states (red) are shown. The light state was generated by irradiation with 50 mW, 120ms pulse duration of 488 nm light prior to collecting each transient spectrum. Data were processed and analyzed using Bruker TopSpin.

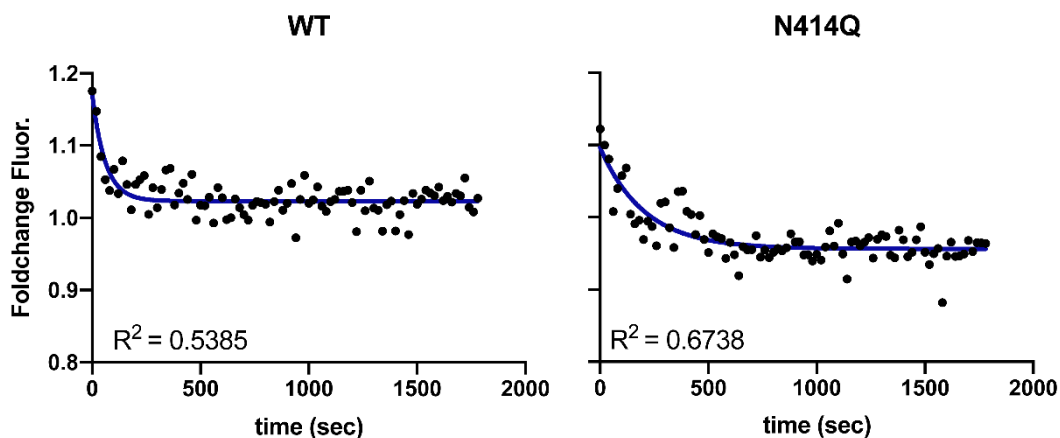


Figure S11: Dark state recovery of AsLOV2 using the LOVTRAP assay. The ΔF signal from after cessation of blue light irradiation from the time trace in **Figure 6** of the main text was fit to a single exponential decay to extract the recovery time of AsLOV2. The readout of ΔF in this assay is directly proportional to recovery (refolding) time of the $J\alpha$ helix rather than recovery of oxidized FMN and is more reflective of protein dynamics. The time constants were determined to be $60 \text{ s} \pm 10 \text{ s}$ and $250 \text{ s} \pm 28 \text{ s}$ for the wild-type and N414Q-AsLOV2 proteins, respectively, which are consistent with recovery times measured in solution using UV-Vis spectroscopy.²¹ N414A-AsLOV2 was not included in this analysis as the curve could not be adequately fit.

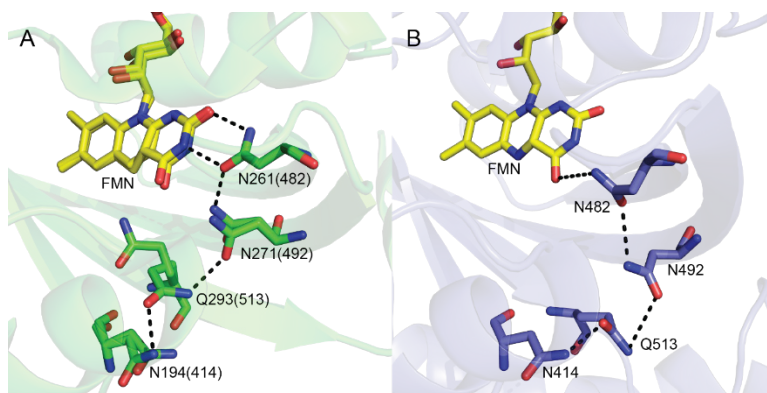


Figure S12: Comparison of 5d-FMN-Aureo and AsLOV2. (A) The crystal structure of the LOV domain of Aureo1a from *Ochromonas Danica* (OdAureo1a, PDB 6I24)²² containing noncanonical FMN analogue, 5-deaza-FMN showed rotation of the conserved Q293(513) and formation of a stable H-bond between the Q293 C=O and the side chain N-H of N194. (B) The 1.15 μ s snapshot from the MD simulation is shown for comparison. Q513 is predicted to be more mobile in the MD simulation and is 3.2 Å further from FMN in the 1.15 μ s snapshot compared to the OdAureo1a structure. The figure was made using the Pymol Molecular Graphics System, Version 1.8, Schrödinger LLC.²⁰

VfAureoI	GDSL I----A QCSPEADTL-----LTDNPSKANRILED PDYSLVKALQMAQQNFVI	221
VIVID	AYQQYHYD-PR TAPTANPLFFHTLYAPGGYDIMGYLIQIMNRPNPQVELGFPVDTSCALIL	75
YtvA	-----MASFQSFGIPGQLEV-----IKKALDHVRVGVVI	29
EL222	QDRPID-----GSGAPGADDT---RVE-VQPPAQWVLDLIEASPIASVV	45
Phy3LOV2	KEKDIPEEDELQELEVIMLEEDASVGRPGSLDDPER----TRR-GIDLATTLERIGKSFVI	933
AsLOV2	PGNI-EKDMLKPRDEDPLLD S-DDERPESFDDELRRKE-MRR-GIDLATTLERIEKNFVI	417
AtLOV2	SNNR-HEDLLRMEPEELMLSTEVIGQRDSDWLSDRERD-IRQ-GIDLATTLERIEKNFVI	393
	: :	::
VfAureoI	TDASLPDNPIVYASRGFLTLTGYSLDQILGRNCRFLQGPET-----DPRAVDKI	270
VIVID	CDLKQKDTPIVYASEAFLYMTGY SNAEVLGRNCRFLQSPDGMVKPKSTRKYVDSNTINTM	135
YtvA	TDPAL EDNPIVYVNGFVQMTGYETEEILGKNCRFLQ GKHT-----DPAEVDNI	78
EL222	SDPRLADNPLIAINQAFTDLTG YSEEECVGRNCRFLAGSGT-----EPWLTDKI	94
Phy3LOV2	TDPRLPDNPIIFASDRFLEL TEYTR EEVLGNNCRFLQGRGT-----DRKAVQLI	982
AsLOV2	TDPRLPDNPIIFASDSFLQLTEYSREEILGRNCRFLQGPET-----DRATVRKI	466
AtLOV2	SDPRLPDNPIIFASDSFLEL TEYSREEILGRNCRFLQGPET-----DQATVQKI	442
	* *.*.: . * : * * : :*.***** . :	:
VfAureoI	RNAITKGVDT SVCLLN YRQDGTTFWNLFVAGLRDSKGNIVNYGVGSKVSE DYAKLLVN	330
VIVID	RKAIDRNAEVQVEVNFKKNQR FVNFLTMI PVRDETGEYRYSMGFCETE-----	186
YtvA	RTALQNKPEPVTVQIQNYKKDGT MFWNELNIDPMEIE--DKTYFVGIQNDITKQKEYEKLL	136
EL222	RQGVREHKPVLVEILNYKKDGT PFRNAV LVAPIYDDDD ELLYFLGSOVEVDDDQPNMGMA	154
Phy3LOV2	RDAVKEQRDVTVQVLNYTKGGRAF WNLFHLQVMRDENG DVQYFIGVQEMVAPRPVHQPP	1042
AsLOV2	RDAIDNQTEVTVQLIN YTKSGKFWNL FHLQPMRDQKGDVQYFIGVQLDGTEH-----VR	521
AtLOV2	RDAIRDQREITVQLIN YTKSGKFWNL FHLQPMRDQKGE LQYFIGVQLDGS DH-----VE	497
	* .: * : * : . * * . : : . : : * * .	
VfAureoI	E--QNIEYKGVRTSNMLRRK-----	348
VIVID	-----	186
YtvA	E--DSLTEITA-----LSTPIVPIRNGISALPLVGNLTE-----ERF---NSIV	175
EL222	R-----RERAAEM-LKTLSPRQ-LEVTTLVASGLRNKEVAARLGLSEKTVKMHRGLV	204
Phy3LOV2	ELPDI LPDRVEQEKA EVVRATAQRV DAAARELPDANLVPD-----HLFAPHSKVV	1092
AsLOV2	DAAE-----REGVMLIKKTAENIDEAAKELPDANLRPE-----DLWANHSKVV	564
AtLOV2	PLQNRLSERTEMQSSKLVKATATNVDEAVREL PDANTRPE-----DLWAAH SKPV	547

Figure S13: Sequence alignment of LOV domain proteins shows variability in N414 position.

Sequences of VfAureoI, VIVID, YtvA, EL222, Phy3LOV2, AsLOV2, and AtLOV2 were aligned using Clustal Omega. The alignment shows that while Q513 is conserved, the N414 position shows variability depending on the LOV domain output.

References:

1. Halavaty, A. S. & Moffat, K. N- and C-terminal flanking regions modulate light-induced signal transduction in the LOV2 domain of the blue light sensor phototropin 1 from *Avena sativa*. *Biochemistry* **46**, 14001–14009 (2007).
2. Pettersen, E. F. *et al.* UCSF Chimera- A visualization system for exploratory research and analysis. *J. Comput. Chem.* **25**, 1605–1612 (2004).
3. Wang, J., Wolf, R. M., Caldwell, J. W., Kollman, P. A. & Case, D. A. Development and testing of a general amber force field. *J. Comput. Chem.* **25**, 1157–1174 (2004).
4. Izadi, S., Anandakrishnan, R. & Onufriev, A. V. Building Water Models: A Different Approach. *J. Phys. Chem. Lett.* **5**, 3863–3871 (2014).
5. Maier, J. A. *et al.* ff14SB: Improving the Accuracy of Protein Side Chain and Backbone Parameters from ff99SB. *J. Chem. Theory Comput.* **11**, 3696–3713 (2015).
6. Jorgensen, W. L., Chandrasekhar, J., Madura, J. D., Impey, R. W. & Klein, M. L. Comparison of simple potential functions for simulating liquid water. *J. Chem. Phys.* **79**, 926–935 (1983).
7. Case, D. A. *et al.* The Amber biomolecular simulation programs. *J. Comput. Chem.* **26**, 1668–1688 (2005).
8. D.A. Case, R.M. Betz, D.S. Cerutti, T.E. Cheatham, III, T.A. Darden, R.E. Duke, T.J. Giese, H. G., A.W. Goetz, N. Homeyer, S. Izadi, P. Janowski, J. Kaus, A. Kovalenko, T.S. Lee, S. LeGrand, P. Li, C., Lin, T. Luchko, R. Luo, B. Madej, D. Mermelstein, K.M. Merz, G. Monard, H. Nguyen, H.T. Nguyen, I., Omelyan, A. Onufriev, D.R. Roe, A. Roitberg, C. Sagui, C.L. Simmerling, W.M. Botello-Smith, J. S. & R.C. Walker, J. Wang, R.M. Wolf, X. Wu, L. X. and P. A. K. Amber 2016.

9. Darden, T., York, D. & Pedersen, L. Particle mesh Ewald: An $N \cdot \log(N)$ method for Ewald sums in large systems. *J. Chem. Phys.* **98**, 10089–10092 (1993).
10. Hopkins, C. W., Le Grand, S., Walker, R. C. & Roitberg, A. E. Long-Time-Step Molecular Dynamics through Hydrogen Mass Repartitioning. *J. Chem. Theory Comput.* **11**, 1864–1874 (2015).
11. Salomon-Ferrer, R., Götz, A. W., Poole, D., Le Grand, S. & Walker, R. C. Routine Microsecond Molecular Dynamics Simulations with AMBER on GPUs. 2. Explicit Solvent Particle Mesh Ewald. *J. Chem. Theory Comput.* **9**, 3878–3888 (2013).
12. Roe, D. R. & Cheatham, T. E. PTRAJ and CPPTRAJ: Software for Processing and Analysis of Molecular Dynamics Trajectory Data. *J. Chem. Theory Comput.* **9**, 3084–3095 (2013).
13. Gil, A. A. *et al.* Femtosecond to Millisecond Dynamics of Light Induced Allostery in the *Avena sativa* LOV Domain. *J. Phys. Chem. B* **121**, 1010–1019 (2017).
14. Harper, S. M., Neil, L. C. & Gardner, K. H. Structural basis of a phototropin light switch. *Science* **301**, 1541–1544 (2003).
15. Greetham, G. M. *et al.* ULTRA: A unique instrument for time-resolved spectroscopy. *Appl. Spectrosc.* **64**, 1311–1319 (2010).
16. Greetham, G. M. *et al.* Time-resolved multiple probe spectroscopy. *Rev. Sci. Instrum.* **83**, 103107 (2012).
17. Fritsch, R. *et al.* Monitoring Base-Specific Dynamics during Melting of DNA–Ligand Complexes Using Temperature-Jump Time-Resolved Infrared Spectroscopy. *J. Phys. Chem. B* **123**, 6188–6199 (2019).
18. Snellenburg, J. J., Laptanok, S. P., Seger, R., Mullen, K. M. & Stokkum, I. H. M. van.

- Glotaran: A Java -Based Graphical User Interface for the R Package TIMP. *J. Stat. Softw.* **49**, (2012).
19. Nash, A. I. *et al.* Structural basis of photosensitivity in a bacterial light-oxygen-voltage/helix-turn-helix (LOV-HTH) DNA-binding protein. *Proc. Natl. Acad. Sci. U. S. A.* **108**, 9449–54 (2011).
 20. The PyMOL Molecular Graphics System, Version 2.0 Schrodinger, LLC.
 21. Zayner, J. P. & Sosnick, T. R. Factors That Control the Chemistry of the LOV Domain Photocycle. *PLoS One* **9**, e87074 (2014).
 22. Kalvaitis, M. E., Johnson, L. A., Mart, R. J., Rizkallah, P. & Allemann, R. K. A Noncanonical Chromophore Reveals Structural Rearrangements of the Light-Oxygen-Voltage Domain upon Photoactivation. *Biochemistry* **58**, 2608–2616 (2019).